


Article

An Ensemble Deep Neural Network-Based Method for Person Identification Using Electrocardiogram Signals Acquired on Different Days

Yeong-Hyeon Byeon ¹ and Keun-Chang Kwak ^{2,*} 

¹ Department of Electrical and Computer Engineering, McGill University, Montreal, QC H3A 0G4, Canada; yeong-hyeon.byeon@mail.mcgill.ca

² Interdisciplinary Program in IT-Bio Convergence System, Department of Electronics Engineering, Chosun University, Gwangju 61452, Republic of Korea

* Correspondence: kwak@chosun.ac.kr; Tel.: +82-062-230-6086

Abstract: Electrocardiogram (ECG) signals are a measure minute electrical signals generated during the cardiac cycle, a biometric signal that occurs during vital human activity. ECG signals are susceptible to various types of noise depending on the data acquisition conditions, with factors such as sensor placement and the physiological and mental states of the subject contributing to the diverse shapes of these signals. When the data are acquired in a single session, the environmental variables are relatively similar, resulting in similar ECG signals; however, in subsequent sessions, even for the same person, changes in the environmental variables can alter the signal shape. This phenomenon poses challenges for person identification using ECG signals acquired on different days. To improve the performance of individual identification, even when ECG data is acquired on different days, this paper proposes an ensemble deep neural network for person identification by comparing and analyzing the ECG recognition performance under various conditions. The proposed ensemble deep neural network comprises three streams that incorporate two well-known pretrained models. Each network receives the time-frequency representation of ECG signals as input, and a stream reuses the same network structure under different learning conditions with or without data augmentation. The proposed ensemble deep neural network was validated on the Physikalisch-Technische Bundesanstalt dataset, and the results confirmed a 3.39% improvement in accuracy compared to existing methods.

Keywords: convolutional neural network; individual identification; electrocardiogram; pretrained neural network; wavelet transform



Citation: Byeon, Y.-H.; Kwak, K.-C. An Ensemble Deep Neural Network-Based Method for Person Identification Using Electrocardiogram Signals Acquired on Different Days. *Appl. Sci.* **2024**, *14*, 7959. <https://doi.org/10.3390/app14177959>

Academic Editors: Tomasz Figlus and Atsushi Mase

Received: 16 July 2024

Revised: 1 September 2024

Accepted: 4 September 2024

Published: 6 September 2024



Copyright: © 2024 by the authors. Licensee MDPI, Basel, Switzerland. This article is an open access article distributed under the terms and conditions of the Creative Commons Attribution (CC BY) license (<https://creativecommons.org/licenses/by/4.0/>).

1. Introduction

An electrocardiogram (ECG) is a bioelectrical signal generated during the cardiac cycle, a process that occurs within the heart during human organ function. To measure the ECG, electrodes are patched onto the skin to amplify minute voltages transmitted from the heart to the skin [1]. Owing to variations in physical attributes, such as weight, height, heart size, muscle mass, and fat mass among individuals, each person exhibits unique characteristic signals. There are several advantages in applying ECG signals for person identification. Using biometric signals such as ECG eliminates the need to remember passwords and reduces the risk of loss or theft associated with keys or ID cards. Moreover, ECG-based identification verifies the user's biometric signal in real time, requiring the user's active participation, and thus preventing proxy authentication. Unlike voice or facial features that can be captured remotely with cameras or recording devices, ECG signals cannot be stored remotely and require the direct attachment of sensors to the skin, offering security advantages by eliminating visual exposure concerns. ECG-based identification has various applications, such as banking transactions via smartphones, unlocking electronic door locks, and website logins [2–8]. Currently, there are non-contact ECG measurement devices

based on the principle of capacitive coupling. However, since ECG signals measure the tiny voltage differences generated by the heart, even non-contact methods are limited to distances of a few millimeters from the skin. Various simplified ECG measurement methods have been developed, such as measuring ECGs by simply touching the wearable watch with the opposite finger while wearing the watch [9,10].

However, ECG signals can be easily distorted by factors such as subject movement during measurement, inevitable breathing, muscle relaxation state, patch placement, and sensor power, among others. To capture high-quality ECG signals, subjects should minimize their movement and remain in a relaxed muscle state. The accurate analysis of ECG data requires expertise in biophysics, and there may be limitations in fully processing the data using computer algorithms alone. As ECG signals contain personal medical information, adherence to data protection regulations is essential. ECG-based identification systems are prone to overfitting the subset of data used in training, making them difficult to generalize to newly collected data [11,12].

Obtaining new ECG signals implies that the electrode patch placement, physical condition, and movements may differ from previous acquisitions, potentially resulting in varying ECG signal shapes even for the same individual. To acquire new ECG signals effectively, it is necessary to do so in a similar environment to ensure stable individual identification based on obtaining similar signals [13–16]. However, achieving consistent patch placement, physical conditions, and movements during each data acquisition attempt is difficult. Different individuals may apply the patches differently, and accurately locating the exact position can be challenging even for the same person. Therefore, using data collected across multiple sessions for training purposes can aid generalization [17–21]. However, such data collection requires additional time and effort [22–24].

The differences in ECG signals, owing to their acquisition in different sessions, pose challenges for neural networks to accurately classify signals. There is less research on handling day-to-day variations in ECG-based biometrics compared to more generalized topics such as domain adaptation and generalization techniques. We investigate ensemble-based networks with the aim of improving generalization. Several studies have explored ensemble methods to classify ECG signals. Yang [25] studied an ensemble classification algorithm based on morphological features to detect abnormalities in ventricular and atrial heart functions. The ECG signals were preprocessed, and waves were detected. The morphological features and principal components of wavelet decomposition were extracted from various ECG segments. Several popular classifiers, including the support vector machine (SVM), k-nearest neighbors (KNN), multilayer perceptron (MLP), AdaBoost, and XGBoost, were considered as components. These components were stacked, and XGBoost was used as the meta-classifier. Essa [26] studied a deep learning-based multi-model system for classifying heart arrhythmias. Two classifiers were investigated: a Convolutional Neural Network-Long Short-Term Memory (CNN-LSTM) and a Long Short-Term Memory (LSTM), utilizing RR intervals and high-order statistics. These classifiers were integrated using a feedforward fully connected neural network as a meta-classifier. Gupta [27] studied local mean decomposition and an ensemble-boosted tree classifier for atrial fibrillation detection using an electrocardiogram. The electrocardiogram was decomposed using local mean decomposition, and four entropy-based features were extracted. The Kruskal–Wallis algorithm was used to calculate the statistical significance of the features. An ensemble-boosted tree classifier was used for classification. Chen [28] studied an ensemble of multiscale convolutional neural networks called EMCNet, to classify electrocardiograms obtained from wearable devices. The EMCNet included two classifier components: an LSTM model using filtered 1D ECG signals and a VGGNet model using time-frequency spectrograms. The prediction probabilities from each classifier were integrated using a weight matrix and softmax layer, resulting in the final prediction outputs. Liu [29] studied an ensemble learning algorithm for detecting atrial fibrillation using single-lead ECG signals obtained from wearable devices. The method comprised three component learners: one utilizing 1D time-series signals, another employing time-frequency spectra, and the third utilizing

Poincaré plots. The outputs from these learners were integrated using a weighted matrix optimized through Bayesian optimization. Kim [30] studied an ensemble network for user recognition using electrocardiograms to prevent overfitting and degradation. Several ECG signals acquired from various user states were used in parallel to train several 1D convolutional neural networks. The outputs of these convolutional neural networks were then integrated and fed into another convolutional neural network to obtain the final results. Sun [31] studied an ensemble multilabel ECG signal classification model using several techniques, including binary relevance, a multilabel hierarchical adaptive resonance associative map, a multilabel twin support vector machine, a classifier chain, a label powerset, an embedder, and embedding. The outputs of each classifier were combined using weights calculated using mutual information and a genetic algorithm. Prabhakararao [32] studied an ensemble of multiple deep convolutional neural networks for arrhythmia classification. Multiple scale-dependent networks were designed with different receptive fields tailored to scale-specific ECG signals. The outputs of these networks were aggregated using the weights calculated using a convolutional gating network. Ihsanto [33] studied ensemble algorithms for detecting driver drowsiness using multiple sensors, including electroencephalograms and ECGs. Logistic regression, a support vector machine, and k-nearest neighbors were used as components, and the final classification was determined using a majority voting classifier. Random forest, which is an ensemble of decision trees, was also considered. Lee [34] studied ensemble algorithms for personal identification using ECG data. The ensemble approach incorporates convolutional neural networks and long short-term memory networks as components. To diversify the models, multiple time-frequency representations were considered, including the short-time Fourier transform, Fourier synchrosqueezed transform, and wavelet synchrosqueezed transform. The outputs of each model were combined using multiplication, and the resulting combined output was used for the final classification.

We conducted research on ensemble deep neural network-based person identification using ECG signals acquired on different days. When acquiring the ECG data in one session, the environmental variables were relatively similar, which resulted in similar ECG signals. However, in different sessions, even for the same individual, changes in environmental variables can alter the shape of the signal, posing challenges for individual identification using ECGs acquired on different days. In simpler terms, performance significantly declines when using data collected on different days for training and validation. Therefore, our research aims to enhance the performance of personal identification using ECG data, even when the data comes from different days. This study proposes an ensemble deep neural network-based model by comparing and analyzing ECG recognition rates under various conditions. The proposed ensemble deep network comprises three streams that incorporate two well-known pretrained models. Each network uses the time-frequency representation of ECG signals as input, and a stream reuses the same network structure under different learning conditions with or without data augmentation. The Physikalisch-Technische Bundesanstalt (PTB) dataset, which consists of data acquired from 15 leads, was used for the experimentation. This includes 12 standard leads and the Frank XYZ leads and encompasses data from 290 individuals, including both healthy subjects and individuals with various heart conditions. The results show that the proposed ensemble deep neural network outperforms existing methods.

This study describes an ensemble deep neural network-based person identification method that uses electrocardiogram signals acquired on different days. Section 2 describes the study methods, and Section 3 presents the ensemble deep neural network-based method for person identification using ECG signals acquired on different days. Section 4 describes the experiments and the results of this study, and Section 5 presents our conclusions.

2. Methods

2.1. Time-Frequency Representation via Continuous Wavelet Transform

A signal that varies over time and consists of a mixture of signals at various frequencies can be decomposed into a time-frequency representation using the continuous wavelet transform. Unlike the Fourier transform, which uses fixed scales regardless of the signal resolution, this method improves efficiency by using scales that vary with the resolution. A continuous wavelet transform decomposes the signal into wavelets of various scales that can reconstruct the signal using a mother wavelet. Equation (1) presents the wavelet transform formula, where $f(t)$ denotes the signal undergoing decomposition, and $\psi_{a,b}(t)$ represents the mother wavelet. The parameter 'a' signifies the scale, while 'b' denotes translation. One notable example among established mother wavelets is the Morse wavelet, as defined in Equation (2) [35–38], which serves as a prominent example.

$$T(a,b) = \frac{1}{\sqrt{a}} \int_{-\infty}^{\infty} f(t) \psi\left(\frac{t-b}{a}\right) dt \quad (1)$$

$a \in \mathbb{R}^+ - \{0\}, b \in \mathbb{R}$

$$\Psi_{P,\gamma}(\omega) = U(\omega) a_{P,\gamma} \omega^{\frac{P}{\gamma}} e^{-\omega^\gamma} \quad (2)$$

$U(\omega)$ is the function of unit step, P^2 represents the time-bandwidth product, $a_{P,\gamma}$ is a normalization factor, and γ is a parameter that controls the symmetry of the Morse wavelet.

2.2. Convolutional Neural Network for Image Classification

Convolutional neural networks (CNNs) have been successfully applied in the field of image pattern recognition. Convolution operations are used to extract features from images, whereas subsampling operations reduce image dimensions while maintaining effective recognition of the image movements. For classification tasks, most CNNs function as classifiers by adding fully connected layers at the end to obtain the final classification results. This structure and mechanism of CNNs automatically learns feature extraction in convolutional layers and effectively trains weights in the final layers for efficient classification of those features. CNN architectures can vary widely through diverse configurations of different layers, and their performances can vary significantly based on these structures. Pretrained models that have already been validated for good performance and trained on massive datasets to optimize weight values can be easily loaded and reused without the complexity of designing from scratch. Pretrained models also efficiently generalize and learn with minimal data and time. Key pretrained models include VGGNet, GoogLeNet, ResNet, Inception-ResNet-v2, DenseNet, and NASNet-Mobile [39–43].

2.3. Preprocessing Methods for ECG Signals

The Pan–Tompkins algorithm is used to detect QRS complexes in ECG signals. The Pan–Tompkins algorithm consists of a series of steps designed to effectively detect QRS complexes in ECG signals. Each step aims to enhance the quality of the ECG signal and accurately identify QRS complexes. It starts with low-pass filtering to reduce noise and high-pass filtering to remove baseline wander and low-frequency noise. Differentiation is then used to highlight the rapid rise and fall of the QRS complex, improving peak detection. A moving average filter is applied to the squared signal to further clarify the QRS locations and reduce noise. Subsequently, QRS locations are detected based on a specific threshold. Finally, verification is performed based on the positions and intervals of the QRS complexes to minimize false detections [44].

The Savitzky–Golay Filter (SGF) [45] is used to suppress high-frequency noise in ECG signals. It generalizes the concept of moving average filters by fitting an n th-order polynomial to the signal values within a window using least-squares and then using the value of the fitted polynomial at the central point of the window as the new smoothed data point.

The Baseline Wandering Path Finding (BWPF) algorithm [46] is used to remove baseline wandering. It uses piecewise polynomial fitting. The ECG signal is divided into multiple segments. The number of segments is specified by the user. The polynomial fitting order is self-assessed based on a threshold value. The algorithm starts with order 1, fits the ECG signal, and computes the fitting error compared to the threshold. If the error exceeds the threshold, the process is repeated with an incremented order until the error is within the acceptable range.

3. Proposed Ensemble Deep Neural Network for Individual Identification Using ECG Signals

This section details the proposed ensemble deep neural network for individual identification using ECG signals. The model comprises three components: a ResNet-based classifier with and without augmentation, and an Inception-ResNet-v2-based classifier.

3.1. First Component for Individual Identification Using ECG

The first component is a ResNet-based classifier that uses the time-frequency representation of an ECG signal as the input. The ECG signal is transformed into a scalogram using a continuous wavelet transform, and this transformed signal is used as an input to train a pretrained ResNet neural network. Additionally, by applying augmentation techniques, the structure of the ResNet remains the same; however, the training data vary, resulting in a newly trained ResNet capable of exploring different features. Figure 1 illustrates an example of transforming an ECG signal into a time-frequency representation using a continuous wavelet transform. Figure 2 shows a ResNet-based classifier for individual identification using ECG signals without data augmentation. Figure 3 shows the ResNet-based classifier for individual identification using ECG signals with data augmentation.

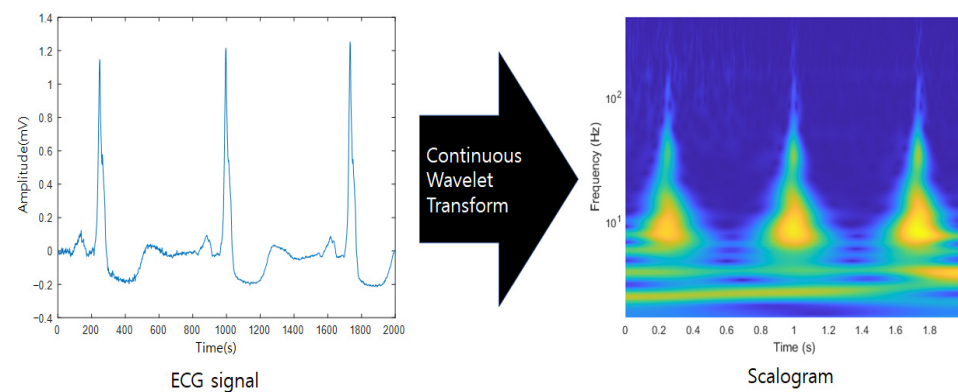


Figure 1. Example of transforming an ECG signal into a time-frequency representation using continuous wavelet transform.

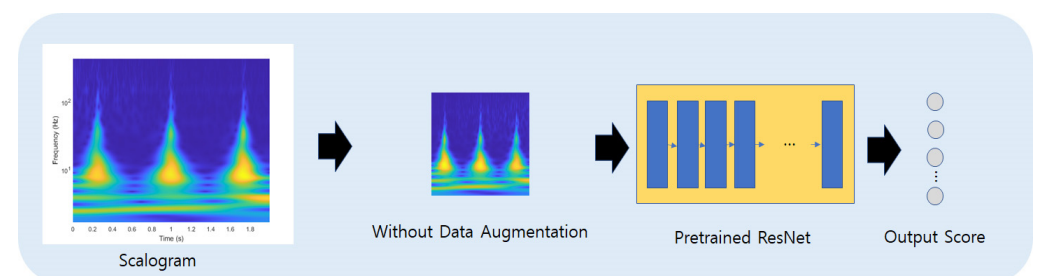


Figure 2. ResNet-based classifier for individual identification using ECG signal without data augmentation.

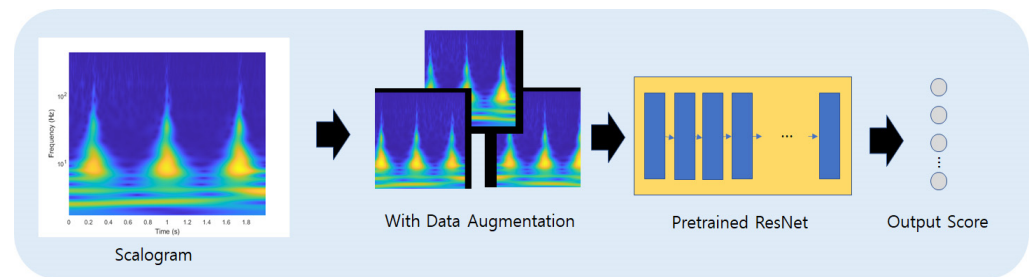


Figure 3. ResNet-based classifier for individual identification using ECG signal with data augmentation.

3.2. Second Component for Individual Identification Using ECG

The second component is an Inception-ResNet-v2-based classifier that uses the time-frequency representation of an ECG signal as input. The ECG signal is transformed into a scalogram using a continuous wavelet transform, and the transformed signal is used as an input to train a pretrained Inception-ResNet-v2 neural network. Figure 4 illustrates the Inception-ResNet-v2-based classifier for individual identification using ECG signals without data augmentation.

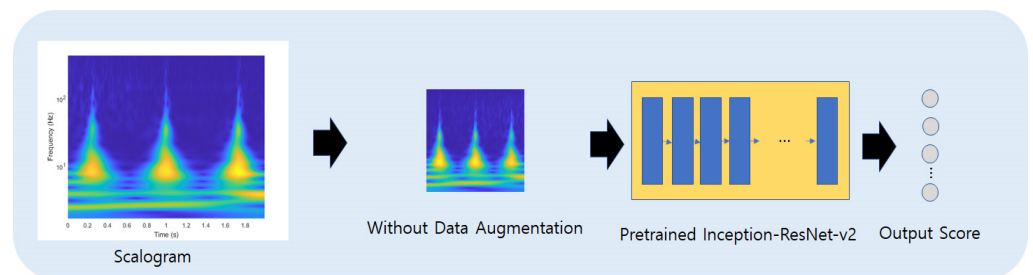


Figure 4. Inception-ResNet-v2-based classifier for individual identification using ECG signals without data augmentation.

3.3. Ensemble Neural Network

The third Ensemble method combines the output scores from multiple classifiers that analyze the same data from various perspectives to reduce overfitting and enhance the robustness of the recognition performance. By integrating scores from multiple classifiers instead of relying on a single neural network, ensemble methods can potentially improve the recognition performance through synergistic effects. Additionally, they offer resilience against misclassifications that may occur in individual networks because corrections from one classifier can complement those from others. Figure 5 illustrates an Ensemble neural network for individual identification using ECG signals, where the output scores of individual classifiers are combined through methods such as multiplication or addition to achieve a unified result. Various pretrained models exist, and these models have been improved through numerous iterations. These pretrained models exhibit performance differences, and achieving better performance by ensembling two models with significantly different performance levels can be challenging. If there is a large performance gap, a less effective model can negatively impact the performance of a better model, reducing overall efficiency. Therefore, this paper uses models with similar performance but different characteristics by reusing models that constitute the ensemble and employing data augmentation. Additionally, it increases the likelihood of exploring different characteristics by leveraging structural differences among the models.

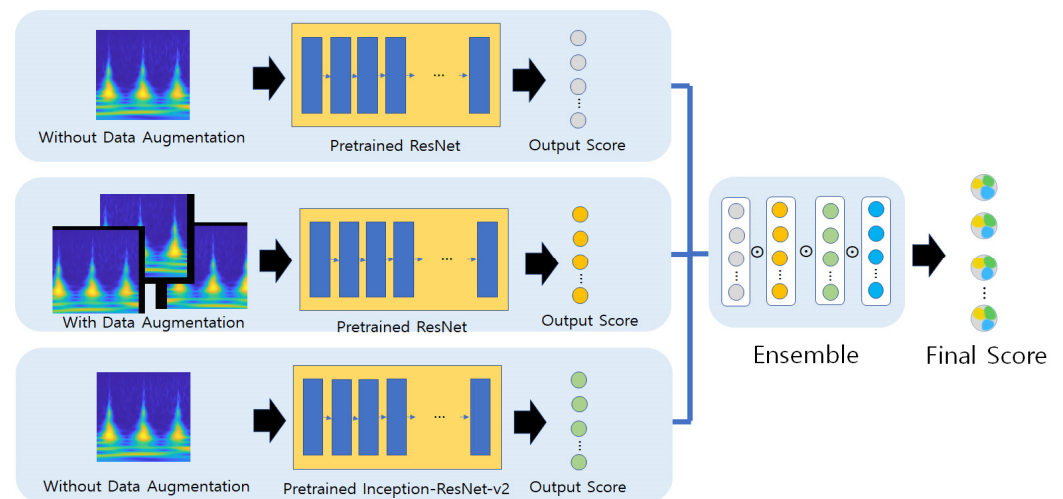


Figure 5. Ensemble neural network for individual identification using ECG signal.

3.4. Evaluation Methods

For performance evaluation, the following metrics were used: Accuracy, Precision, Recall, F1-Score, False Rejection Rate (FRR), and False Acceptance Rate (FAR). Accuracy measures the proportion of correctly identified instances among all instances. Precision indicates the proportion of correctly identified positive instances of all predicted positive instances. Recall measures the ratio of correctly identified positive instances to all actual positive instances. F1-Score is the harmonic mean of the precision and recall, providing a balance between the two metrics. The FRR is the proportion of genuine acceptances that are incorrectly rejected. The FAR is the proportion of impostor attempts that are incorrectly accepted. These metrics are commonly used in classification tasks to assess the performance of the classifiers based on their predictions and true data labels. These evaluation methods are calculated using the following formulas based on True Positives (TP), False Positives (FP), True Negatives (TN), and False Negatives (FN) [47]:

$$\text{Accuracy} = \frac{\text{TP} + \text{TN}}{\text{TP} + \text{TN} + \text{FP} + \text{FN}} \quad (3)$$

$$\text{Precision} = \frac{\text{TP}}{\text{TP} + \text{FP}} \quad (4)$$

$$\text{Recall} = \frac{\text{TP}}{\text{TP} + \text{FN}} \quad (5)$$

$$\text{F1-Score} = \frac{2 \times (\text{Precision} \times \text{Recall})}{\text{Precision} + \text{Recall}} \quad (6)$$

$$\text{FRR} = \frac{\text{FP}}{\text{FP} + \text{TN}} \quad (7)$$

$$\text{FAR} = \frac{\text{FN}}{\text{TP} + \text{FN}} \quad (8)$$

We have essentially trained the network to improve accuracy and are making performance improvements accordingly. Since precision, sensitivity, and other metrics are also important for personal identification, they have been included as well.

4. Experiments and Results

4.1. ECG Datasets for Individual Identification

The PTB electrocardiogram (ECG) database was used to evaluate the performance of the proposed methodology. The PTB-ECG database comprises 549 high-resolution ECG recordings obtained from 290 patients. This dataset includes both healthy individuals

and patients presenting various cardiac pathologies. The recordings were acquired from 15 leads, including 12 standard leads and the Frank XYZ leads. Participants' ages ranged from 17 to 87 years, comprising 209 males and 81 females. Data for each subject were acquired in the form of 1–5 record files. The ECG signals were sampled at 1000 samples/s with a 16-bit resolution. Each record included medical summaries containing age, sex, and diagnostic information. PTB-ECG encompasses nine diagnostic categories, including various cardiac conditions, as shown in Figure 6 [48,49].

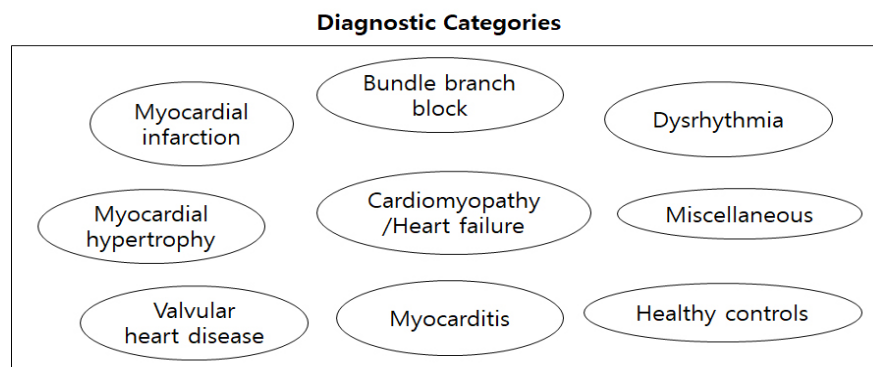


Figure 6. Diagnostic categories of the PTB-ECG dataset.

4.2. Experiments and Results

To perform the experiments, this study used a computer equipped with an Intel® (Santa Clara, CA, USA) Core(TM) i7-10700 CPU @ 2.9 GHz, Windows 10 64 bit, 8 GB RAM (Random Access Memory), an NVIDIA GeForce RTX 2060, and Matlab 2023b.

To train and validate the data from the same session, the PTB dataset was utilized and the Pan–Tompkins algorithm was used to detect the R-peaks. Subsequently, the segments centered around these detected R-peaks were extracted to ensure equal sizes before and after each peak. For ECG signals with a sample length of 2000, each segment was constructed to include 1000 samples before and after the R-peak. Data for which the number of detected R-peaks did not meet a certain threshold were excluded. A total of 239 individuals were included, with 70 samples allocated for training and 30 for validation for each individual. The training dataset consisted of 16,730 samples (239 subjects \times 70 samples) and the validation dataset consisted of 7170 samples (239 subjects \times 30 samples).

To train and validate the data from the different sessions, only data from individuals who had at least two sessions available were selected from the PTB dataset. The Pan–Tompkins algorithm was employed to detect the R-peaks and ensure the segments centered around the detected R-peaks of equal sizes before and after each peak was extracted. For the ECG signals with a sample length of 2000, each segment consisted of 1000 samples before and after the R-peak. Data for which the number of detected R-peaks did not meet a certain threshold were excluded. A total of 105 individuals were selected, with 70 and 30 samples allocated for training and validation, respectively, per individual. The training dataset consisted of 7350 samples (105 subjects \times 70 samples), and the validation dataset consisted of 3150 samples (105 subjects \times 30 samples).

Table 1 presents the experimental results of the training and validation of data from the same session. The ECG signals were transformed into time-frequency representations using a continuous wavelet transform, and the pretrained ResNet-101 was trained. The mini-batch size was 30, with a maximum of 20 epochs, and an initial learning rate of 0.0001, with no data augmentation being used. Adam optimization was employed. Single 1-channel ECG signals from the PTB dataset were used in this study. For a noise reduction comparison between pre- and post-processing, high-frequency noise was filtered using SGF with the parameters set to polynomial order 0 and frame length 15. Baseline wandering was addressed using BWPF, with parameters configured for 30 segments.

Table 1. Experimental results when training and validating with data from the same session.

Sample Length	Filtering	Accuracy (%)	Precision (%)	Recall (%)	F1-Score (%)	FRR (%)	FAR (%)
1500	-	98.58	98.87	98.58	98.53	0.01	1.42
2000	-	99.48	99.52	99.48	99.48	0.00	0.52
3000	SGF, BWPF	98.94	99.13	98.94	98.88	0.01	1.06

Table 2 presents the experimental results when training and validating the data from different sessions. The ECG signals were transformed into time-frequency representations using a continuous wavelet transform, and the pretrained ResNet-101 was trained. The mini-batch size was 30, with a maximum of 20 epochs, and an initial learning rate of 0.0001, with no data augmentation being used. Adam optimization was employed. The ECG signal had a sample length of 800, and the experimental results are shown for the input data from the 1-channel, 2-channel, and 3-channel ECG signals from the PTB dataset.

Table 2. Experimental results when training and validating using data from different sessions.

Sample Length	ECG Channel	Accuracy (%)	Precision (%)	Recall (%)	F1-Score (%)	FRR (%)	FAR (%)
800	1	49.27	54.19	49.27	53.14	0.95	50.73
800	2	47.27	50.97	47.27	51.77	1.04	52.73
800	3	42.25	45.03	42.25	51.37	1.26	57.75

Table 3 shows the experimental results of training and validation with data from different sessions without cutting the ECG signals precisely at the R-peak positions, but instead finely overlapping segments and training the neural network models regardless of the starting point of the data. The ECG signals were transformed into Mel-spectrograms, and a CNN-LSTM neural network model was trained. For the Mel-spectrogram transformation, a window length of 256 and hop length of 64 were applied, with 128 bands. The CNN-LSTM architecture consists of three sets of Convolution-BatchNorm-ReLU-MaxPool layers and one LSTM layer. The convolution filters were sized three, with 64, 64, and 128 filters applied. The LSTM had 256 hidden nodes. A mini-batch size of 32, maximum training epochs of 20, and initial learning rate of 0.005 were used, with Adam optimization. The segment and hop sizes listed in Table 3 were used to shorten the long ECG signals for the input size.

Table 3. Experimental results of training and validating with data from different sessions without cutting the ECG signals precisely at R-peak positions.

Signal Segment Size	Signal Hop Size	Accuracy (%)
800	10	22.80
800	50	20.74

Table 4 presents the experimental results based on the sample lengths of the ECG signals during training and validation using data from different sessions. The ECG signals were transformed into time-frequency representations using a continuous wavelet transform, and the pretrained ResNet-101 was trained. The mini-batch size was 30, with a maximum of 20 epochs, and an initial learning rate of 0.0001, with no data augmentation being used. Adam optimization was also applied. Figure 7 shows examples of signals with various sample lengths. We validated the data for different days using a signal with a single cycle. However, due to the low recognition rate, we expected that increasing the signal length would improve performance. To observe this, we conducted experiments by

gradually increasing the input signal at regular intervals. The reason we can only estimate the results of this nonlinear recognition rate is that the portions of the signal being cut varied, and the signal was ambiguously truncated in the middle, which may have led to a reduction in the contributions of highly recognized parts of the signal throughout the data. Other possible reasons are an increase of unnecessary information and a reduction in the resolution of the input data to cover a broad range of the signal. We aimed to find the optimal length through experimental repetition.

Table 4. Experimental results on the effect of sample length of ECG signals when training and validating using data from different sessions.

Sample Length	Accuracy (%)	Precision (%)	Recall (%)	F1-Score (%)	FRR (%)	FAR (%)
1500	49.94	52.99	49.94	55.52	0.94	50.06
2000	55.08	54.23	55.08	59.13	0.77	44.92
3000	48.95	50.07	48.95	51.65	0.97	51.05

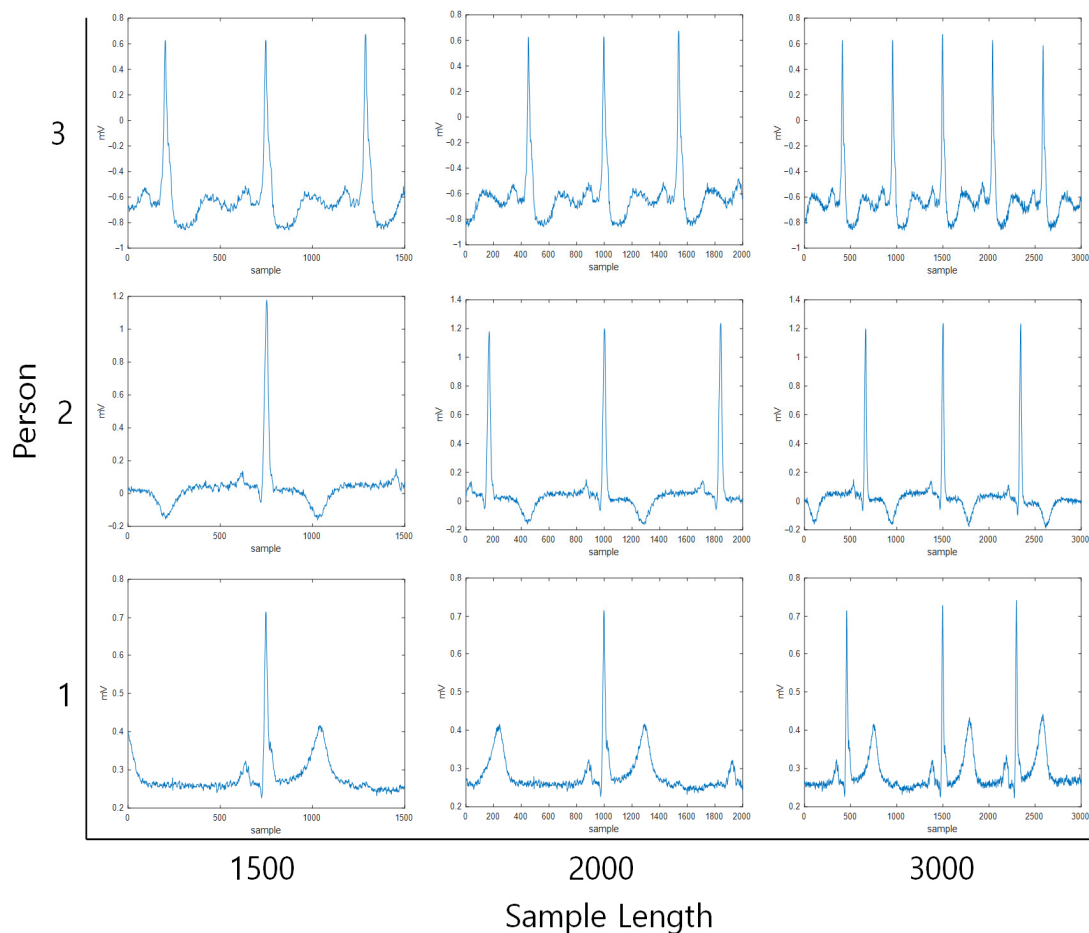
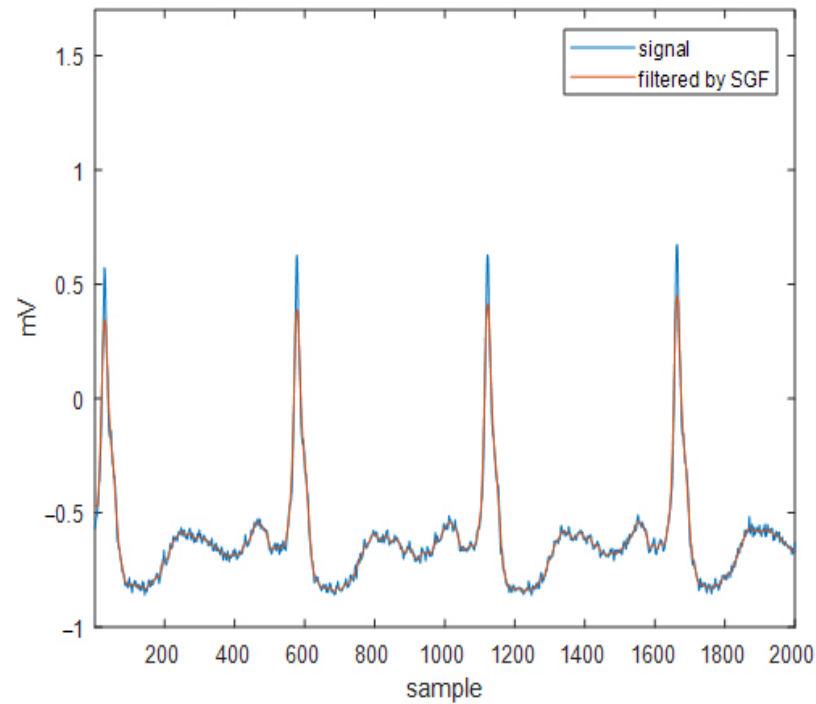


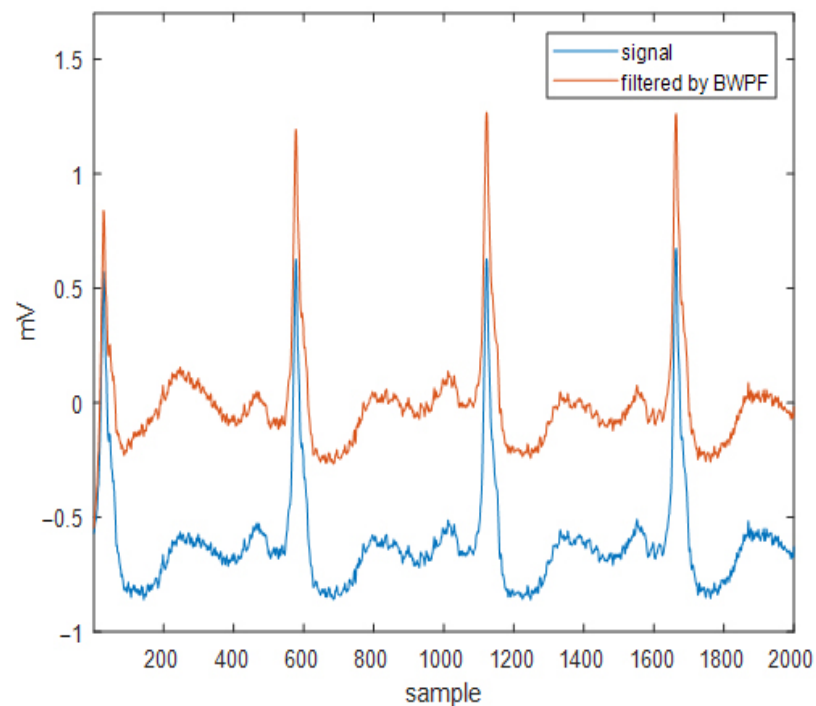
Figure 7. The examples of signals with various sample lengths.

Table 5 presents the experimental results of the effects of noise reduction during training and validation using data from different sessions. The ECG signals were transformed into time-frequency representations using a continuous wavelet transform, and the pretrained ResNet-101 was trained. The mini-batch size was 30 with a maximum of 20 epochs, and an initial learning rate of 0.0001, with no data augmentation being used. Adam optimization was also applied. It is observed that BWPF does not affect accuracy,

while the SGF is observed to significantly reduce accuracy. Figure 8 shows the results of the SGF and BWPF of an ECG signal. If the SGF's polynomial order is higher, it is closer to the original signal, and if the SGF's frame length is shorter, it is also closer to the original signal. We set the parameters to minimize distortion of the signals while providing a slight smoothing effect intuitively. The most distorted part of SGF is observed in QRS complexes. The result of filtering can be improved by adjusting the other SGF's parameters, but the result will be very similar to the original signal.



(a) SGF



(b) BWPF

Figure 8. The results of applying the SGF and BWPF on an ECG signal.

Table 5. Experimental results on the effects of noise reduction during training and validation using data from different sessions.

Sample Length	Filtering	Accuracy (%)	Precision (%)	Recall (%)	F1-Score (%)	FRR (%)	FAR (%)
2000	SGF, BWPF	13.71	41.18	13.71	18.09	4.01	86.29
2000	SGF	16.48	50.81	16.48	21.70	2.26	83.52
2000	BWPF	55.65	56.41	55.65	58.30	0.75	44.35
3000	SGF, BWPF	13.05	45.41	13.05	16.27	3.84	86.95

Table 6 presents the experimental results of the effects of the sample length when applying only BWPF during training and validation using data from different sessions. The ECG signals were transformed into time-frequency representations using a continuous wavelet transform, and the pretrained ResNet-101 was trained. The mini-batch size was 30, with a maximum of 20 epochs, and an initial learning rate of 0.0001, with no data augmentation being used. Adam optimization was also applied.

Table 6. Experimental results on the effects of sample length when applying only BWPF during training and validation using data from different sessions.

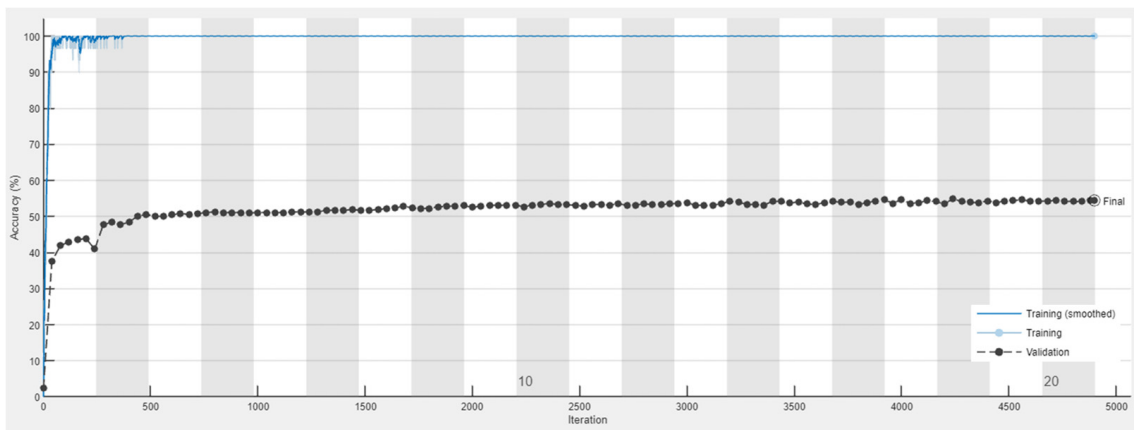
Sample Length	Filtering	Accuracy (%)	Precision (%)	Recall (%)	F1-Score (%)	FRR (%)	FAR (%)
1500	BWPF	45.59	52.76	45.59	50.32	1.11	54.41
2000	BWPF	55.65	56.41	55.65	58.30	0.75	44.35
3000	BWPF	54.95	55.19	54.95	58.43	0.77	45.05

Table 7 presents the experimental results for the effect of expanding the input channels for the ECG signals during training and validation using data from different sessions. The ECG signals were transformed into time-frequency representations using a continuous wavelet transform, and the pretrained ResNet-101 was trained. The mini-batch size was 30, with a maximum of 20 epochs, and an initial learning rate of 0.0001, with no data augmentation being used. Adam optimization was also applied.

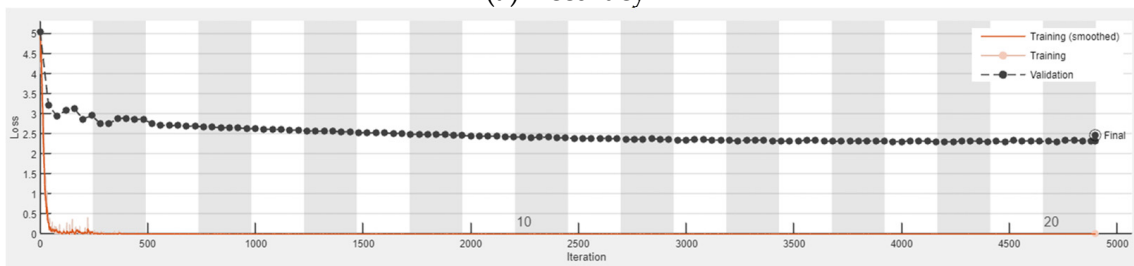
Table 7. Experimental results on the effect of expanding input channels for ECG signals during training and validation using data from different sessions.

Sample Length	ECG Channel	Accuracy (%)	Precision (%)	Recall (%)	F1-Score (%)	FRR (%)	FAR (%)
2000	1 + 2	46.95	49.13	46.95	52.07	1.05	53.05
2000	1 + 2 + 3	48.16	53.35	48.16	53.81	1.00	51.84

Table 8 presents the experimental results for various single pretrained models when training and validating using data from different sessions. The ECG signals were transformed into time-frequency representations using a continuous wavelet transform. The models trained included pretrained ResNet-101, pretrained ResNet-101 with augmentation, and pretrained Inception-ResNet-v2. The mini-batch size was 30, with a maximum of 20 epochs, an initial learning rate of 0.0001, and Adam optimization. Figures 9–11 depict the training processes of each pretrained deep neural network when training and validating with data from different sessions. As shown in the figures, the validation utilized 20% of the test set.

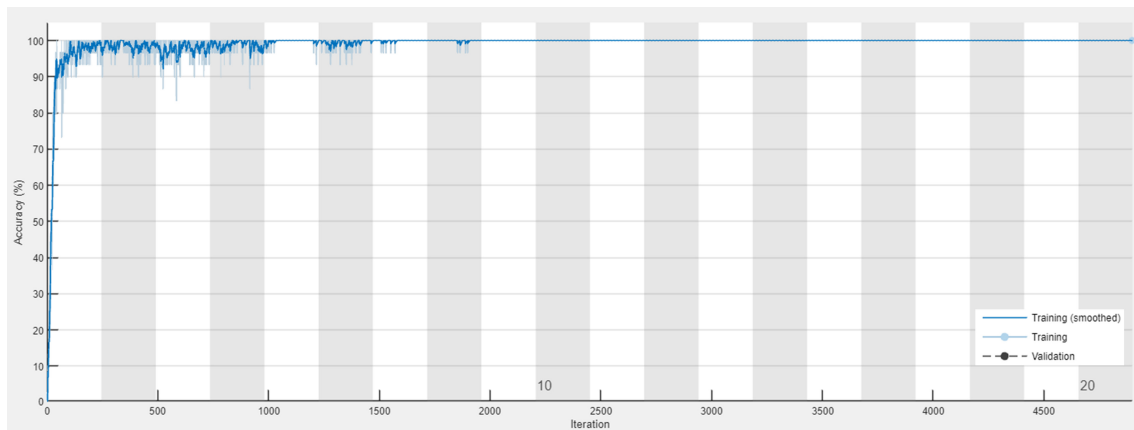


(a) Accuracy

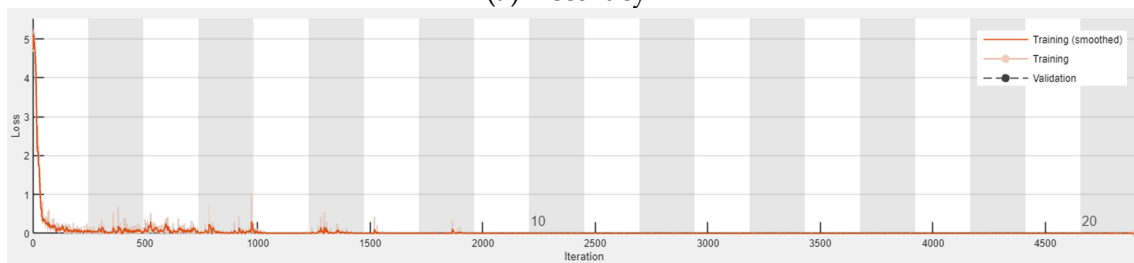


(b) Loss

Figure 9. Training processes of pretrained ResNet-101 when training and validating with data from different sessions.



(a) Accuracy



(b) Loss

Figure 10. Training processes of pretrained ResNet-101 with data augmentation when training and validating with data from different sessions.

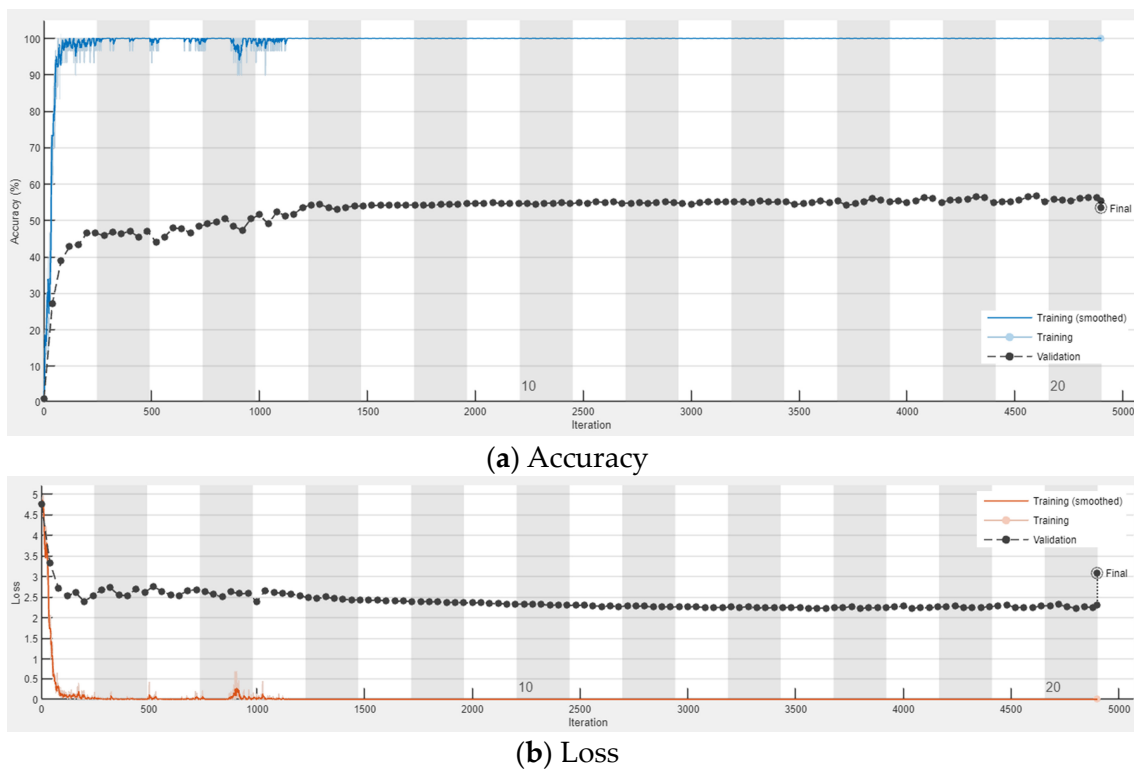


Figure 11. Training processes of pretrained Inception-ResNet-v2 when training and validating with data from different sessions.

Table 8. Experimental results on various single pretrained models when training and validating using data from different sessions.

Sample Length	Method	Accuracy (%)	Precision (%)	Recall (%)	F1-Score (%)	FRR (%)	FAR (%)
2000	ResNet-101	55.08	54.23	55.08	59.13	0.77	44.92
2000	ResNet-101(aug)	56.22	56.35	56.22	59.50	0.73	43.78
2000	Inception-ResNet-v2	54.67	56.55	54.67	57.15	0.78	45.33

Table 9 presents the experimental results of the ensemble deep neural network trained and validated using data from different sessions. By combining the output scores of individual deep neural networks through addition and multiplication operations, we designed Ensemble Deep Network-Plus (EDNet-P) and Ensemble Deep Network-Multiplication (EDNet-M). The EDNet-P and -M are ensemble deep neural networks that combine the outputs of three pretrained models: ResNet, ResNet with augmentation, and Inception-ResNet-v2, using addition and multiplication, respectively. In terms of accuracy, the proposed EDNets showed at least a 2.57% improvement compared with the single models.

Table 9. Experimental results of ensemble deep neural network when training and validating with data from different sessions.

Sample Length	Method	Accuracy (%)	Precision (%)	Recall (%)	F1-Score (%)	FRR (%)	FAR (%)
2000	EDNet-P	58.79	58.71	58.79	61.26	0.66	41.21
2000	EDNet-M	59.11	60.05	59.11	60.73	0.65	40.89

Table 10 shows the experimental results of various network combinations when training and validating with data from different sessions. The reason performance can be improved is due to the complementary interactions between the networks' final scores. For example, suppose Net-A accurately classifies people 1 through 10 but poorly classifies people 11 through 20, while Net-B poorly classifies people 1 through 10 but accurately classifies people 11 through 20. Although each network might show similar poor performance individually, if Net-A and Net-B interact appropriately, they could collectively classify people 1 through 20 more effectively. From the perspective of the networks' output scores, even if Net-B assigns a relatively high score to the 5th person, who is actually the 1st person, Net-A is likely to assign a lower score to the 5th person. Therefore, combining their scores would reduce the likelihood of classifying the 1st person as the 5th person. The reason why the performance of some network combinations does not improve significantly is that these combinations fail to complement each other's relative weaknesses. This study explores individual network characteristics through experimental repetition.

Table 10. Experimental results of various network combinations when training and validating with data from different sessions.

Combination of Models	Fusion Method	Accuracy (%)
ResNet, ResNet(aug)	Multiplication	57.68
ResNet, ResNet(aug)	Additon	58.25
ResNet(aug), Inception-ResNet-v2	Multiplication	56.32
ResNet(aug), Inception-ResNet-v2	Addition	55.94
ResNet, Inception-ResNet-v2	Multiplication	58.38
ResNet, Inception-ResNet-v2	Addition	57.52

Here, we investigated the experimental results of other methods. Table 11 shows the experimental results of other methods when training and validating with data from different sessions. The CZE-SVM utilized cepstral coefficients, zero crossing rate, and entropy for feature engineering, and several support vector machines were used for classification [50]. The EECGNet was designed based on PCANet. PCANet is a cascaded linear network that uses principal component analysis (PCA) filters for convolutions. The outputs are binarized, combined with weights, and then used to calculate histograms. The final results are obtained through the following process [51]: EECGNet-1 is configured with three stages, a patch size of three, four filters, and a block overlap rate of 0.5. EECGNet-2 is configured with four stages, a patch size of five, four filters, and a block overlap rate of 0.5. EECGNet-3 is configured with four stages, a patch size of seven, four filters, and a block overlap rate of 0.5. The EDNet showed more higher accuracies than other methods. We tested the CZE-SVM using code obtained from the author's open repository [52]. It exhibited very poor accuracy, ranging from 13.19% to 17.75%. The method performed inadequately in normalizing ECG signals that vary from day to day. Other methods also demonstrated poor accuracy with day-to-day variations in ECG signals, even after applying a band-pass filter. EECGNet has shown accuracy rates ranging from 39.37% to 55.40%. There are significant accuracy gaps depending on its parameter settings. There are many parameters; therefore, we were able to explore only a limited set of parameters. Compared to the accuracies shown in Table 9, our EDNet-P and EDNet-M methods achieve at least 3.39% higher accuracy than the other methods.

Table 11. Experimental results of other methods when training and validating with data from different sessions.

Sample Length	Method	Noise Reduction	Accuracy (%)
2000	CZE-Linear-SVM [50]	-	17.75
2000	CZE-Polynomial-SVM [50]	-	12.73
2000	CZE-Rbf-SVM [50]	-	15.71
T-to-T wave	CZE-Linear-SVM [50]	-	14.37
T-to-T wave	CZE-Polynomial-SVM [50]	-	12.16
T-to-T wave	CZE-Linear-SVM [50]	-	13.19
2000	CZE-Linear-SVM [50]	Band Pass Filter	0.98
2000	CZE-Polynomial-SVM [50]	Band Pass Filter	0.98
2000	CZE-Rbf-SVM [50]	Band Pass Filter	1.30
2000	EECGNet-1 [51]	-	55.40
2000	EECGNet-2 [51]	-	45.68
2000	EECGNet-3 [51]	-	39.37

Table 12 shows the experimental results of EECGNet [51] under various parameters. Some training trials with parameters are failed due to the memory lack issue. There are possibilities that other methods can be more robust by adjusting the parameters. There are many parameters; therefore, we were able to explore only a limited set of parameters.

Table 12. Experimental results of EECGNet [51] under various parameters.

Stage	Patch-Size	Filter Number	Hist Block Size	Block Overlap Rate	Accuracy
1	3	6	3, 3	0.5	49.17
2	3, 3	3, 3	3, 3	0.5	47.94
2	3, 3	6, 6	3, 3	0.5	54.44
2	3, 3	3, 3	7, 7	0.5	48.44
3	3, 3, 3	4, 4, 4	3, 3	0.5	55.37
3	7, 7, 7	6, 6, 6	7, 7	0.3	47.33
3	7, 7, 7	6, 6, 6	7, 7	0.5	47.59

To enhance model interpretability, methods such as a class activation map have been proposed. In this paper, the ensemble approach, which uses multiple independent models, offers the possibility of interpretation across various features without relying solely on a single model's interpretation. Additionally, by incorporating separate subnetworks for interpretation within the ensemble, it is anticipated that the decision-making process can be further analyzed in the future.

When performing personal identification using data collected on the same day, a fairly high recognition rate is achieved. In this paper, only data from one day was used for training, but it is expected that increasing the number of days in the training data will further improve the recognition rate. Although the recognition rate was 59.11% when using data from one day for training and data from other days for validation, it is anticipated that further improvements will allow for accurate personal identification while reducing the variability of training data acquisition.

5. Conclusions

We conducted an ensemble deep neural network-based person identification using ECG signals collected on different days. ECG signals capture minute electrical impulses produced during the cardiac cycle and serve as biometric signals during human activity. These signals are susceptible to various types of noise depending on the data acquisition conditions, including sensor placement and the subject's physiological and mental state, resulting in diverse signal shapes. During a single session of data acquisition, the environmental variables remained relatively constant, leading to consistent ECG signals. However, across multiple sessions, environmental changes can alter the signal morphology, posing challenges for ECG-based person identification over different days. To address this issue, this study proposed an ensemble deep neural network that evaluates and compares ECG recognition performance under diverse conditions. The ensemble deep neural network comprised three streams that incorporate two established pretrained models. Each network stream takes the time-frequency representation of ECG signals as input, with one stream reusing the same network architecture under varied learning conditions, including with and without data augmentation. The ensemble included ResNet-101 and Inception-ResNet-v2 as stream members. Experimental validation was conducted using the PTB dataset, demonstrating that the proposed ensemble deep neural network resulted in a 3.39% performance enhancement in accuracy compared to existing methodologies. This approach, while potentially increasing model stability by learning various features independently, requires more computing and time resources. Although the recognition rate was low when using ECG data from different days for validation, including data from multiple sessions in the training set is expected to improve the recognition rate. In future research, we will explore the robust features extracted from ECG signals acquired on different days and investigate ensemble methods to integrate these features more effectively.

Author Contributions: Conceptualization, Y.-H.B. and K.-C.K.; Methodology, Y.-H.B. and K.-C.K.; Software, Y.-H.B. and K.-C.K.; Validation, Y.-H.B. and K.-C.K.; Formal Analysis, Y.-H.B. and K.-C.K.; Investigation, Y.-H.B. and K.-C.K.; Resources, K.-C.K.; Data Curation, K.-C.K.; Writing—Original Draft Preparation, Y.-H.B.; Writing—Review and Editing, K.-C.K.; Visualization, Y.-H.B. and K.-C.K.; Supervision, K.-C.K.; Project Administration, K.-C.K.; Funding Acquisition, K.-C.K. All authors have read and agreed to the published version of the manuscript.

Funding: This research was supported by the Basic Science Research Program of the National Research Foundation of Korea (NRF) funded by the Ministry of Education (No. 2017R1A6A1A03015496).

Institutional Review Board Statement: Not applicable.

Informed Consent Statement: Not applicable.

Data Availability Statement: Data are available in a publicly accessible repository. The data presented in this study are openly available in PhysioNet at <https://www.physionet.org/content/ptbdb/1.0.0/> (accessed on 10 June 2024), reference number [48].

Conflicts of Interest: The authors declare no conflicts of interest.

References

1. Gahi, Y.; Lamrani, M.; Zoglat, A.; Guennoun, M.; Kapralos, B.; El-Khatib, K. Biometric Identification System Based on Electrocardiogram Data. In Proceedings of the New Technologies, Mobility and Security, Tangier, Morocco, 5–7 November 2008; pp. 1–4.
2. Boles, W.W. A Security System Based on Human Iris Identification Using Wavelet Transform. In Proceedings of the First International Conference on Conventional and Knowledge Based Intelligent Electronics Systems, Adelaide, Australia, 21–23 May 1997; pp. 533–541.
3. Zhang, Y.; Juhola, M. On biometrics with eye movements. *IEEE J. Biomed. Health Inform.* **2017**, *21*, 1360–1366. [CrossRef]
4. Wang, H.; Hu, J.; Deng, W. Compressing fisher vector for robust face recognition. *IEEE Access* **2017**, *5*, 23157–23165. [CrossRef]
5. Jain, A.K.; Arora, S.S.; Cao, K.; Best-Rowden, L.; Bhatnagar, A. Fingerprint recognition of young children. *IEEE Trans. Inf. Forensics Secur.* **2017**, *12*, 1505–1514. [CrossRef]
6. Mobarakeh, A.K.; Carrillo, J.A.C.; Aguilar, J.J.C. Robust face recognition based on a new supervised kernel subspace learning method. *Symmetry* **2019**, *19*, 1643. [CrossRef] [PubMed]

7. Pokhriyal, N.; Tayal, K.; Nwogu, I.; Govindaraju, V. Cognitive-biometric recognition from language usage: A feasibility study. *IEEE Trans. Inf. Forensics Secur.* **2017**, *12*, 134–143. [[CrossRef](#)]
8. Nguyen, B.P.; Tay, W.L.; Chui, C.K. Robust biometric recognition from palm depth images for gloved hands. *IEEE Trans. Hum.-Mach. Syst.* **2015**, *45*, 799–804. [[CrossRef](#)]
9. Wang, T.-W.; Lin, S.-F. Negative impedance capacitive electrode for ecg sensing through fabric layer. *IEEE Trans. Instrum. Meas.* **2021**, *70*, 4002308. [[CrossRef](#)]
10. Wang, X.; Liu, S.; Zhu, M.; He, Y.; Wei, Z.; Wang, Y.; Xu, Y.; Pan, H.; Huang, W.; Chen, S.; et al. Flexible non-contact electrodes for wearable biosensors system on electrocardiogram monitoring in motion. *Front. Neurosci.* **2022**, *16*, 900146. [[CrossRef](#)]
11. Patwary, A.B.; Chowdhury, M.T.I.; Mamun, N. Comparison among ECG filtering methods for non-linear noise. In Proceedings of the International Conference on Advancement in Electrical and Electronic Engineering, Gazipur, Bangladesh, 22–24 November 2018; p. 141.
12. Lee, E.; Ho, A.; Wang, Y.-T.; Huang, C.-H.; Lee, C.-Y. Cross-Domain Adaptation for Biometric Identification Using Photoplethysmogram. In Proceedings of the IEEE International Conference on Acoustics, Speech and Signal Processing, Barcelona, Spain, 4–8 May 2020; pp. 1289–1293.
13. Nazi, Z.A.; Biswas, A.; Rayhan, M.A.; Abir, T.A. Classification of ECG signals by dot residual LSTM network with data augmentation for anomaly detection. In Proceedings of the International Conference on Computer and Information Technology, Dhaka, Bangladesh, 18–20 December 2019; pp. 1–5.
14. Chang, C.-H.; Wang, T.-M.; Hsu, H.L. Denoising of mixed noises in ecg with separate noise estimators based on discrete wavelet transform. In Proceedings of the IEEE International Conference on Advanced Materials for Science and Engineering, Tainan, Taiwan, 12–13 November 2016; pp. 562–564.
15. Satija, U.; Ramkumar, B.; Manikandan, M.S. Automated ECG noise detection and classification system for unsupervised healthcare monitoring. *IEEE J. Biomed. Health Inform.* **2018**, *22*, 722–732. [[CrossRef](#)]
16. Xu, X.; Cai, Q.; Wang, H.; Suo, Y.; Zhao, Y.; Tianwei, W.; Wang, G.; Lian, Y. A 12-Lead ECG Delineation Algorithm Based on a Quantized CNN-BiLSTM Auto-Encoder with 1–12 mapping. In Proceedings of the International Conference on Artificial Intelligence Circuits and Systems, Hangzhou, China, 11–13 June 2023; pp. 1–5.
17. Yang, H.; Liu, J.; Zhang, L.; Li, Y.; Zhang, H. ProEGAN-MS: A progressive growing generative adversarial networks for electrocardiogram generation. *IEEE Access* **2021**, *9*, 52089–52100. [[CrossRef](#)]
18. Anwar, T.; Zakir, S. Effect of image augmentation on ECG image classification using deep learning. In Proceedings of the International Conference on Artificial Intelligence, Islamabad, Pakistan, 5–7 April 2021; pp. 182–186.
19. Choi, S.; Seo, H.-C.; Cho, M.S.; Joo, S.; Nam, G.-B. Performance improvement of deep learning based multi-class ECG classification model using limited medical dataset. *IEEE Access* **2023**, *11*, 53185–53194.
20. Cayce, G.I.; Depoian, A.C., II; Bailey, C.P.; Guturu, P. Improved neural network arrhythmia classification through integrated data augmentation. In Proceedings of the IEEE MetroCon, Hurst, TX, USA, 3 November 2022; pp. 1–3.
21. Li, J.; Wang, G.; Chen, M.; Ding, Z.; Yang, H. Mixup asymmetric tri-training for heartbeat classification under domain shift. *IEEE Signal Process. Lett.* **2021**, *28*, 718–722. [[CrossRef](#)]
22. Bazi, Y.; Alajlan, N.; AlHichri, H.; Malek, S. Domain adaptation methods for ECG classification. In Proceedings of the International Conference on Computer Medical Applications, Sousse, Tunisia, 22 April 2013; pp. 1–4.
23. Rafi, T.H.; Ko, Y.W. Heartnet: Self multihead attention mechanism via convolutional network with adversarial data synthesis for ECG-based arrhythmia classification. *IEEE Access* **2022**, *10*, 100501–100512. [[CrossRef](#)]
24. Alawad, M.; Wang, L. Learning domain shift in simulated and clinical data: Localizing the origin of ventricular activation from 12-lead electrocardiograms. *IEEE Trans. Med. Imaging* **2019**, *38*, 1172–1184. [[CrossRef](#)] [[PubMed](#)]
25. Yang, H.; Wei, Z. A novel approach for heart ventricular and atrial abnormalities detection via an ensemble classification algorithm based on ecg morphological features. *IEEE Access* **2021**, *9*, 54757–54774. [[CrossRef](#)]
26. Essa, E.; Xie, X. An ensemble of deep learning-based multi-model for ecg heartbeats arrhythmia classification. *IEEE Access* **2021**, *9*, 103452–103464. [[CrossRef](#)]
27. Gupta, K.; Bajaj, V.; Ansari, I.A. Atrial fibrillation detection using electrocardiogram signal input to lmd and ensemble classifier. *IEEE Sens. Lett.* **2023**, *7*, 7002904. [[CrossRef](#)]
28. Chen, J.; Li, H.; Zhang, L.-B.; Teng, Y.; Fortino, G. Emcnet: Ensemble multiscale convolutional neural network for single-lead ecg classification in wearable devices. *IEEE Sens. J.* **2024**, *24*, 8754–8762. [[CrossRef](#)]
29. Liu, Y.; Fang, B.; Chen, Y.; Lv, Z. Ensemble learning-based atrial fibrillation detection from single lead ecg wave for wireless body sensor network. *IEEE Trans. Netw. Sci. Eng.* **2023**, *10*, 2627–2636. [[CrossRef](#)]
30. Kim, M.-G.; Choi, C.; Pan, S.B. Ensemble networks for user recognition in various situations based on electrocardiogram. *IEEE Access* **2019**, *8*, 36527–36535. [[CrossRef](#)]
31. Sun, Z.; Wang, C.; Zhao, Y.; Yan, C. Multi-label ecg signal classification based on ensemble classifier. *IEEE Access* **2020**, *8*, 117986–117996. [[CrossRef](#)]
32. Prabhakararao, E.; Dandapat, S. Multi-scale convolutional neural network ensemble for multi-class arrhythmia classification. *IEEE J. Biomed. Health Inform.* **2022**, *26*, 3802–3812. [[CrossRef](#)] [[PubMed](#)]
33. Gwak, J.; Hirao, A.; Shino, M. An investigation of early detection of driver drowsiness using ensemble machine learning based on hybrid sensing. *Appl. Sci.* **2020**, *10*, 2890. [[CrossRef](#)]

34. Lee, J.-A.; Kwak, K.-C. Personal identification using an ensemble approach of 1d-lstm and 2d-cnn with electrocardiogram signals. *Appl. Sci.* **2022**, *12*, 2692. [[CrossRef](#)]
35. Lilly, J.M.; Olhede, S.C. On the analytic wavelet transform. *IEEE Trans. Inf. Theory* **2010**, *56*, 4135–4156. [[CrossRef](#)]
36. Lilly, J.M.; Olhede, S.C. Generalized Morse wavelets as a superfamily of analytic wavelets. *IEEE Trans. Signal Process.* **2012**, *60*, 6036–6041. [[CrossRef](#)]
37. Olhede, S.C.; Walden, A.T. Generalized morse wavelets. *IEEE Trans. Signal Process.* **2002**, *50*, 2661–2670. [[CrossRef](#)]
38. Lilly, J.M.; Olhede, S.C. Higher-order properties of analytic wavelets. *IEEE Trans. Signal Process.* **2009**, *57*, 146–160. [[CrossRef](#)]
39. Szegedy, C.; Liu, W.; Jia, Y.; Sermanet, P.; Reed, S.; Anguelov, D.; Erhan, D.; Vanhoucke, V.; Rabinovich, A. Going deeper with convolutions. In Proceedings of the IEEE Conference on Computer Vision and Pattern Recognition, Boston, MA, USA, 7–12 June 2015; pp. 1–9.
40. Simonyan, K.; Zisserman, A. Very deep convolutional neural networks for large-scale image recognition. In Proceedings of the International Conference on Learning Representations, San Diego, CA, USA, 7–9 May 2015; pp. 1–14.
41. He, K.; Zhang, X.; Ren, S.; Sun, J. Deep residual learning for image recognition. In Proceedings of the IEEE Conference on Computer Vision and Pattern Recognition, Las Vegas, NV, USA, 27–30 June 2016; pp. 770–778.
42. Szegedy, C.; Loffe, S.; Vanhoucke, V.; Alemi, A.A. Inception-v4, inception-resnet and the impact of residual connections on learning. In Proceedings of the AAAI Conference on Artificial Intelligence, San Francisco, CA, USA, 4–9 February 2017; pp. 4278–4284.
43. Zoph, B.; Vasudevan, V.; Shlens, J.; Le, Q.V. Learning transferable architectures for scalable image recognition. In Proceedings of the IEEE/CVF Conference on Computer Vision and Pattern Recognition, Lake City, UT, USA, 18–23 June 2018; pp. 8697–8710.
44. Pan, J.; Tompkins, W.J. A real-time qrs detection algorithm. *IEEE Trans. Biomed. Eng.* **1985**, *BME-32*, 230–236. [[CrossRef](#)]
45. Schafer, R.W. What is a savitzky-golay filter? [lecture notes]. *IEEE Signal Process. Mag.* **2011**, *28*, 111–117. [[CrossRef](#)]
46. Rahman, M.A.; Milu, M.M.H.; Anjum, A.; Khanam, F.; Ahmad, M. Baseline wandering removal from ecg signal by wandering path finding algorithm. In Proceedings of the 3rd International Conference on Electrical Information and Communication Technology, Khulna, Bangladesh, 7–9 December 2017; pp. 1–5.
47. Choi, H.S.; Lee, B.H.; Yoon, S.R. Biometric authentication using noisy electrocardiograms acquired by mobile sensors. *IEEE Access* **2016**, *4*, 1266–1273. [[CrossRef](#)]
48. Goldberger, A.L.; Amaral, L.N.; Glass, L.; Hausdorff, J.M.; Ivanov, P.C.; Mark, R.G.; Mietus, J.E.; Moody, G.B.; Peng, C.K.; Stanley, H.E. PhysioBank, PhysioToolkit, and PhysioNet: Components of a new research resource for complex physiologic signals. *Circulation* **2000**, *101*, e215–e220. [[CrossRef](#)]
49. Wubbelier, G.; Stavridis, M.; Kreiseler, D.; Boussejot, R.D.; Elster, C. Verification of humans using the electrocardiogram. *Pattern Recognit. Lett.* **2007**, *28*, 1172–1175. [[CrossRef](#)]
50. Hamza, S.; Ayed, Y.B. An integration of features for person identification based on the pqrst fragments of ecg signals. *Signal Image Video Process.* **2022**, *16*, 2037–2043. [[CrossRef](#)]
51. Lee, J.-N.; Byeon, Y.-H.; Pan, S.-B.; Kwak, K.-C. An eigenecg network approach based on pcanet for personal identification from ecg signal. *Sensors* **2018**, *18*, 4024. [[CrossRef](#)] [[PubMed](#)]
52. Github-Senum. Available online: <https://github.com/Senum/Person-identification-using-ECG> (accessed on 10 July 2024).

Disclaimer/Publisher’s Note: The statements, opinions and data contained in all publications are solely those of the individual author(s) and contributor(s) and not of MDPI and/or the editor(s). MDPI and/or the editor(s) disclaim responsibility for any injury to people or property resulting from any ideas, methods, instructions or products referred to in the content.